ANNALS OF GEOPHYSICS, 68, 3, NS332, 2025; doi:10.4401/ag-9126
OPEN ACCESS

Seismic Response Study Around the Bridge of the Lions, Chapultepec Forest, México City

Martín Cárdenas-Soto[*,1], David Escobedo-Zenil[1], Jesús Sánchez-González[1], Martín Carlos Vidal-García[1]

[(1)] National Autonomous University of Mexico, School of Engineering, Geophysical Department, Mexico City, México

Article history: received July 18, 2024; accepted October 19, 2024

Abstract

The Bridge of the Lions, with its straps resting on two artificial slopes, serves as a pedestrian walkway for hundreds of Mexico City residents who visit the Chapultepec Forest daily. Ambient seismic noise results let us explain the bridge deterioration, a direct result of the local terrain subsidence. The site frequency, measured in the free field (1.14 Hz), matches the estimate on the bridge straps, indicating that the strap depth does not reach the firm layer. At 1.72 Hz, the bridge vibrates more vertically. This frequency is close to site frequency, suggesting soil-structure interaction effects. Also, the rotating analysis of HVSR functions in the bridge straps revealed a second peak of 1.64 Hz caused by vibration from the Av. Circuito Interior vehicle flow. The spectral analysis of virtual source sections obtained by the seismic Interferometry technique reveals that superficial materials have velocities similar to soft clays in the lake area (Vs < 150 m/s). A second layer of poorly consolidated clays (Vs 350 m/s) with significant lateral variation indicates that subsidence around the bridge is causing significant damage to the structure. According to this study, soil-structure interaction effects are present, as the bridge foundations likely do not penetrate the most competent deep strata. This suggests that additional inquiry is necessary to assess the static and seismic response of the bridge.

Keywords: HVSR; Seismic Interferometry; Surface Waves; Lake Zone; Land Subsidence

1. Introduction

The change in the subsoil conditions is caused by its compaction due to the loss of saturation, which happens in many cities because of groundwater extraction (Galloway et al., 1998; Motagh et al., 2017). The pore pressure decreases during periods of water production, the mean confining pressure acting on the soil increases (Anochikwa, et al., 2012), and as a result, the soft soil deposit experiences severe compaction, which results in the accumulation of both plastic and elastic strains. Because of this, any subsequent increase in the water table will only result in a partial recovery of the initial compaction (Tarantino and De Col, 2008). Over many cycles, the soil deposit will continuously accrue a considerable amount of settlement (Durazo and Farvolden, 1989), ultimately leading to a permanent sinking that requires monitoring and mitigation for sustainable development.

In Mexico City, land subsidence has resulted in the structural deterioration of historical monuments and buildings (Ovando et al., 2008; Avíles and Pérez Rocha, 2010; Auvinet et al., 2017). The fracturing is a clear indication of the local subsidence of lake sequences, which sink over time due to the exploitation of the aquifer of the Mexico City

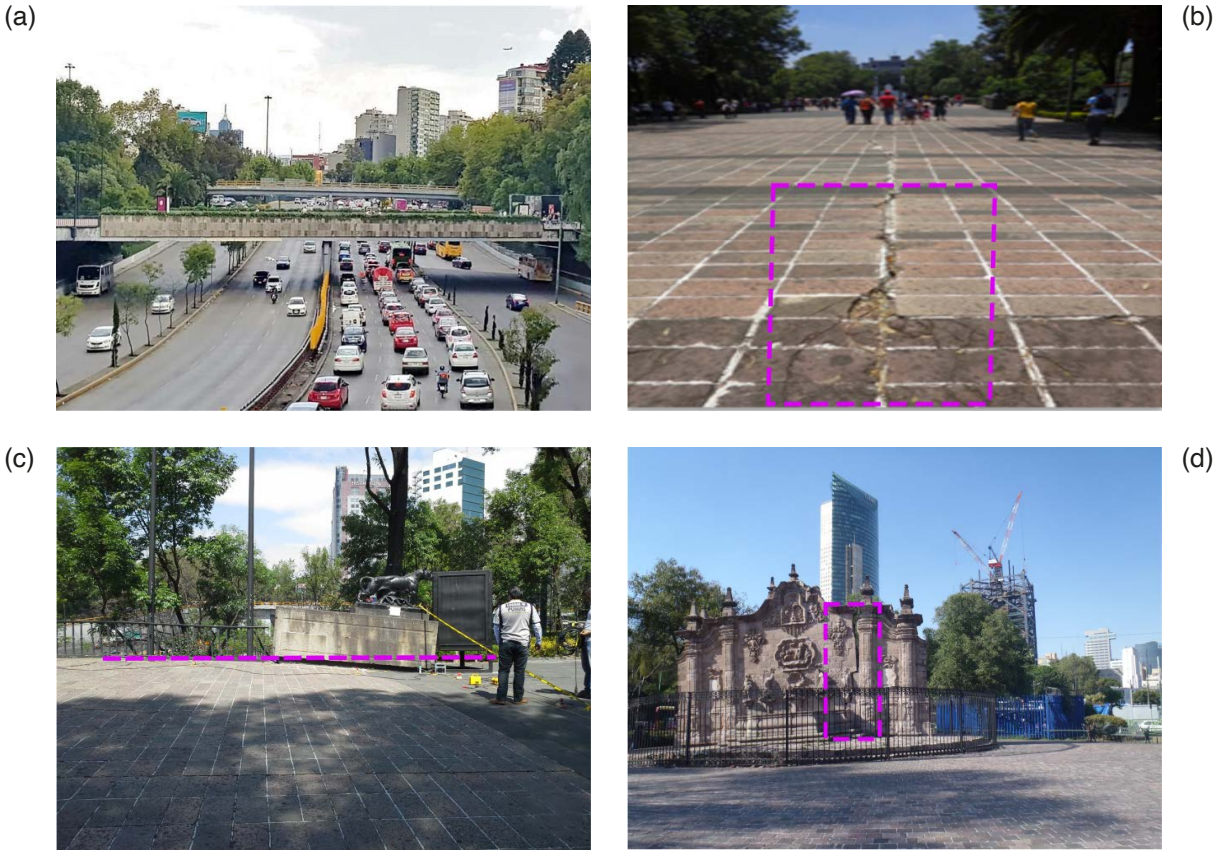

Figure 1. Details of the identified surface features of Bridge of the Lions: (a) south side view of the bridge, (b) fracturing along the bridge parapet, (c) inclination of one of the lion monuments at the northern end of the bridge, and (d) cracking of the monument Fuente de Belen.

Basin (Auvinet et al., 2013; Figueroa-Miranda et al., 2018). The subsidence phenomenon continues at an average rate of 36 cm/year, with accumulated values resulting in differential sinkings of up to 9 m (Cabral-Cano et al., 2008; Cigna and Tapete, 2021). The effects of subsidence are particularly severe in transition zones, where lake deposits intersect with volcanic material, leading to serious threats to urban infrastructure. One of the most iconic sites in Mexico City, located in the transition zone, is the Chapultepec Forest. This forest is of great importance due to its historical and cultural sites (Gobierno de México, 2022). The First Section of the forest is characterized by the historic Chapultepec Castle, the zoo, and the lake area. The effects of subsidence around the Bridge of the Lions (whose foundations blocks rest on artificial slopes, see Fig. 1) are evident in fractures with lengths ranging from 2 to 8 m, sinkings along Juventud Heroica Avenue, and deterioration of the perimeter fence. The subsidence is also observed near the access to the Chapultepec metro station, with the most severe damage occurring in the historical monument called Fuente de Belen, which marks the beginning of the ancient Chapultepec Aqueduct (Fig. 1).

In a comprehensive study, we conducted seismic response and subsoil structure analysis around the Bridge of the Lions. The objective is to examine the effects of local terrain subsidence utilizing ambient seismic noise methodologies and identify vulnerabilities to prevent future degradation and ensure the safety and stability of the Bridge. Ambient seismic noise experiments were conducted, characterizing the site response using the HVSR (Horizontal to Vertical Spectral Ratio) method and Fourier amplitude spectra. Additionally, the S wave velocity structure was determined through surface waves extracted from the cross-correlation of seismic noise, providing a detailed understanding of the subsoil conditions.

2. Study site and experiments

The artificial slopes of Av. Juventud Heroica are situated in a transitional zone with a change in relief. It consists of volcanic deposits from the Tarango formation, which are part of the lake deposits of the Valley of Mexico. Geotechnical

surveys were used to establish the stratigraphy for the construction of the monument Estela de Luz, located on one side of the Gate of the Lions, and built in 2011 to commemorate the bicentennial of independence of Mexico from Spanish authority. According to these surveys, the lake sequence has a thickness of 31.90 m, with a hard layer of 5.2 m between depths of 23.60 and 28.80 m. Below this, there are alluvial sands, limes, sands, and pumitic and andesitic gravel characteristic of the Tarango formation, with a thickness from 31.90 to 65.20 m. These materials dominate the seismic response of the site, with a fundamental frequency of about 1 Hz in geotechnical lake zone called IIIa.

In this study, we thoroughly examined the subsoil structure and the vibration state of the Bridge of Lions. We used ambient seismic noise in two frequency ranges, for frequencies below 4.5 Hz, we recorded an hour of seismic noise at 12 points in the open field and 7 points on the bridge using triaxial seismometers model CMG-6TD from Guralp Systems. For frequencies above 4.5 Hz, we recorded an hour of seismic noise in three arrays with vertical geophones connected to Seistronix seismographs model EX12. The data were collected between the years of 2013 and 2014 as part of a project to explore the subsoil. In this study, these arrays were used to generate 2D images of Vs by spectral analysis of surface waves extracted from the cross-correlation between pairs of receivers. Figure 2 shows the location of the arrays and the measurement points of ambient noise.

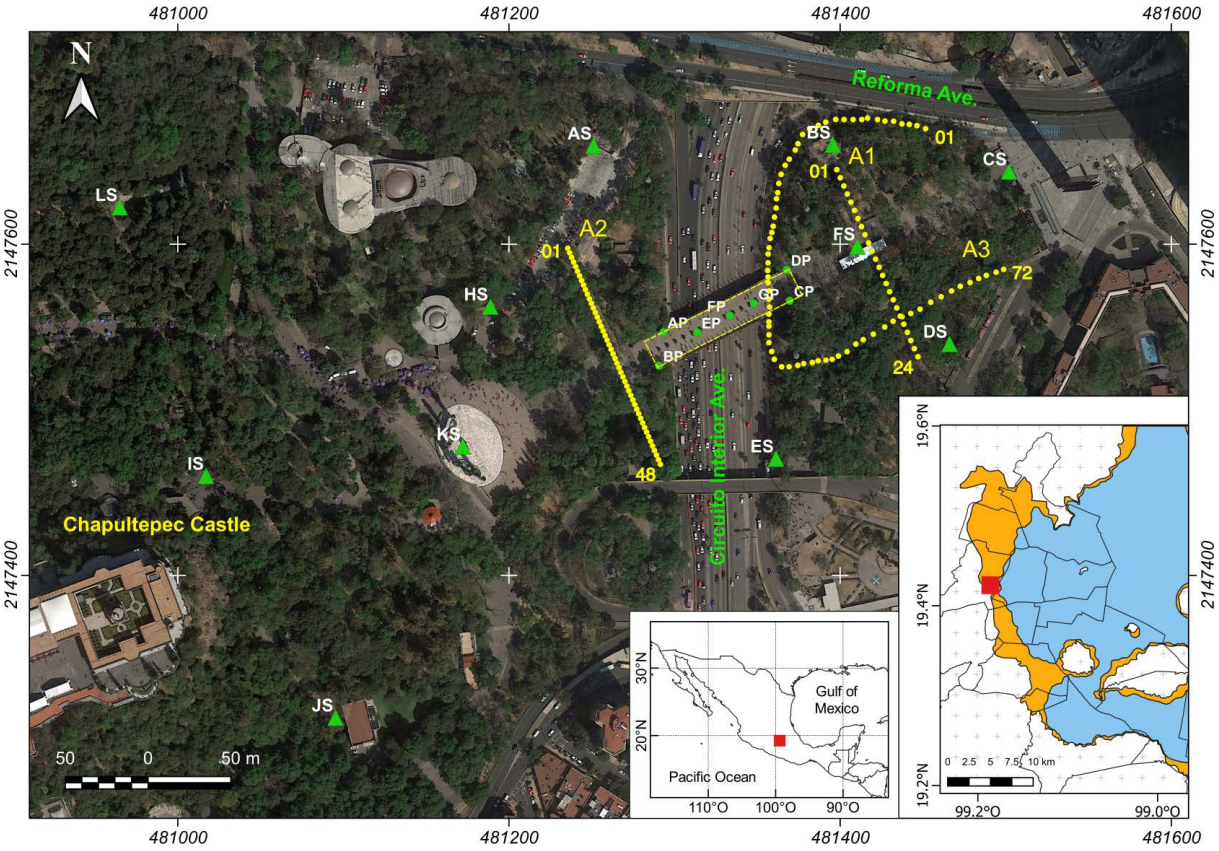

Figure 2. Locations where ambient seismic noise was recorded. The green symbols with white letters represent triaxial seismometers, while the yellow circles indicate the vertical geophone arrays A1, A2, and A3. The initial and final geophone number is indicated at each array. The yellow discontinuous line rectangle outlines the perimeter of the Bridge of the Lions. A red square indicates the location of the research area in the embedded figures. The lake and transition geotechnical zones, delineated by the isoperiod curve of 1 s, are shown in blue and orange on the Mexico City map, respectively. (Image adapted from Google Earth®).

3. Seismic response in the free field

The HVSR technique (Nakamura, 1989; Lermo and Chávez-García, 1993) allows us to measure seismic site effects, which is the relative amplification of soil due to the presence of soft soil and the frequency at which this amplification

occurs. It is widely acknowledged that the ambient vibration signals utilized to derive HVSRs typically arise from both body and surface waves, with the latter often being predominant (e.g. Bonnefoy-Claudet et al., 2006). The ratios of the horizontal to vertical components of body waves propagating vertically through the soil deposit can be interpreted as the site transfer function. However, this does not apply to surface waves that include both Rayleigh and Love waves. If ambient noise is dominated by Rayleigh waves, the H/V ratio may approximate the ellipticity of the particle motion induced by these surface waves (e.g. Tuan et al., 2011). Conversely, if Love waves dominate, the maximum of the H/V ratio corresponds to the Airy phase, as noted by Konno and Ohmachi (1998). In both instances, the frequency position of the fundamental resonance peak of the soil deposit is nearly identical; however, the HVSR method does not yield an accurate amplification factor (see also Bonnefoy-Claudet et al., 2008). Subsequently, we examine the seismic site response and do the computations of the HVSR curves without investigating the characteristics of the seismic noise field. We analyze and address the resonance peak about the soil deposit that generates it to identify discrepancies between the site response in the free field and the subsoil beneath the bridge foundation.

During one hour of recording, we obtained an average spectral ratio from 60 s duration windows without overlap. The result was the arithmetic average of the two horizontal components (Wathelet et al., 2008). Figure 3 displays the average HVSRs of all measurement points. The IS, BS, and FS points have amplitudes less than 6. The IS point, located at the foot of Chapultepec Hill, does not exhibit site effects. The spectral ratio at the BS station indicates that the seismic response is caused by a weak impedance contrast between the soft layers and the substratum. The high noise level induced by the Reforma and Circuito Interior avenues likely caused the measurement not to align with the average curves of the other sites. The FS station, located at the center of the hole, shows an apparent site effect with an average amplitude of 5 at the average frequency of 1 Hz, which differs from nearby measurement points (CS, DS, and ES). Notably, the response at DS has an amplitude twice the size of two nearby sites (CS and ES) located 100 meters away. This indicates that the seismic response varies laterally at very short distances, reflecting the non-homogeneity of surface materials in that area (Cárdenas-Soto et al., 2021).

We will assume that the spectral ratios depicted in Fig. 3 represent the one-dimensional response of a soft soil layer. It is important to note that we have not investigated the characteristics and composition of surface waves in the context of seismic noise, and the shape of the HVSR curves likely indicates a more intricate nature of site response. The depth of the substratum can be estimated using the formula f0 = β/4H, where f0 represents the resonance frequency of the soil layer, β denotes the shear velocity, and H indicates the thickness of the layer. The average site frequency is observed to be 1.1 Hz. Considering an average wave velocity of 100 m/s, which will be determined in the subsequent section, a depth of 23 m is calculated. This depth is consistent with the findings reported in the geotechnical study of the Estela de Luz (TGC, 2010).

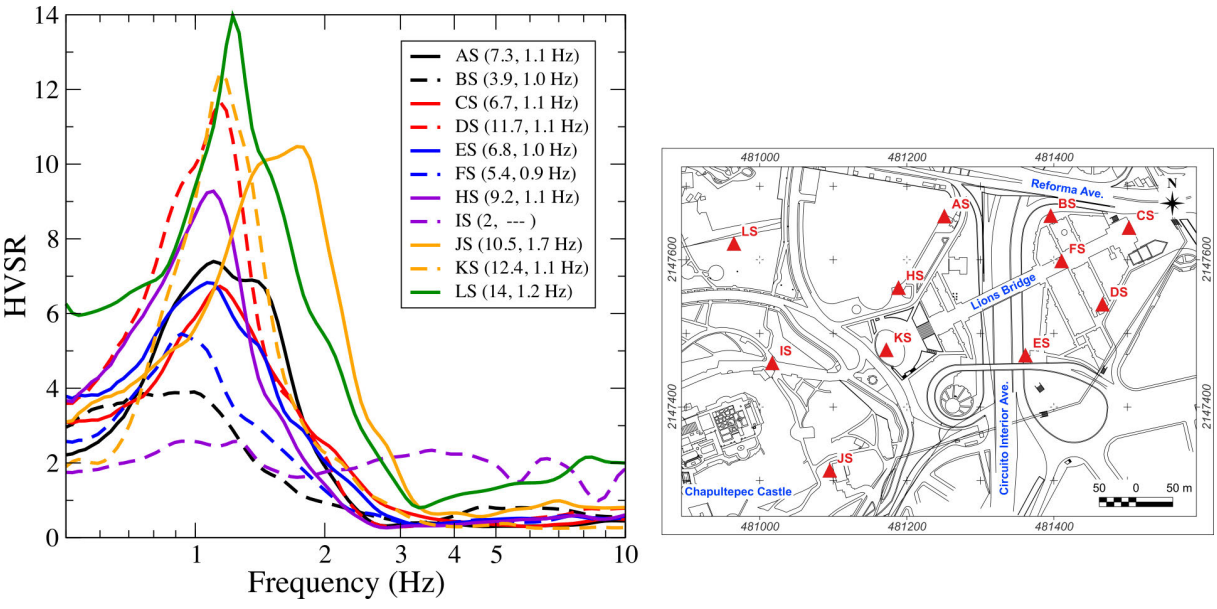

Figure 3. Average Horizontal-to-Vertical Spectral Ratio (HVSR) curves for each recording point at the triaxial stations (red rectangles in the location map). The values in parentheses indicate the maximum relative amplitude of the HVSR curve and the frequency at which it occurs.

4. Vibration analysis on the bridge

To assess the seismic response of the bridge, we examined the ambient noise vibration records at each instrumented point on the bridge structure (see Fig. 2). Figure 4 displays the HVSRs at the vertices of the bridge (points AP, BP, CP, and DP) and at deck central points EP, FP and GP. The HVSRs at the vertices indicate a frequency of 1.14 Hz with an average relative amplitude of 6. At the FP station, the fundamental frequency is 1.09 Hz with a relative amplitude of 4. These frequency values are similar to those found at open-field sites (Fig. 2), indicating that the bridge foundation is located on soft soil deposits. Moreover, at points BP and DP, a second spectral peak is observed at a frequency of 1.64 Hz, while point FP exhibits a minimum at 1.72 Hz. Now, if we calculate the Fourier amplitude spectra of the points on the bridge slab (EP and GP points), we will obtain the frequency of vibrating of this one. The average amplitude spectra (obtained from 60 windows of 60 s duration) of the vertical components at the EP and GP points are also shown in Fig. 4. In that figure, the fundamental mode and three higher modes of vibrating of the structure are clearly observed: 1.72, 2.40, 3.66, and 6.11 Hz, respectively. The amplitude spectra of the horizontal components of those points did not exhibit any vibration frequency, indicating that the bridge vibrates mainly in the vertical direction.

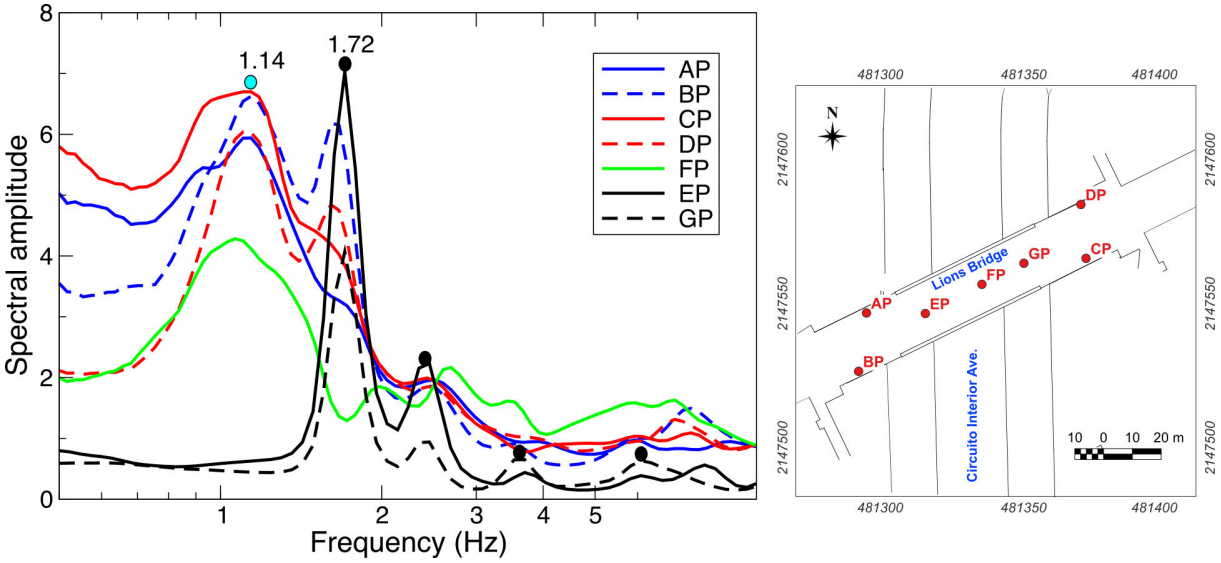

Figure 4. HVSR curves (red and green lines) and Fourier amplitude spectra on the vertical component (black lines) of ambient vibration recording points on the Bridge of Lions (red circles in the location map). The cyan color circle indicates the dominant frequency of the HVSRs (1.14 Hz), and the black circles indicate the vibration frequencies of the bridge, whose fundamental frequency is 1.72 Hz.

The fundamental mode frequency of the bridge is 1.72 Hz, which is very close to the second spectral maximum of 1.64 Hz observed in the HVSR of the BP and DP points. Additionally, the value of 1.72 Hz corresponds to the minimum HVSR curve of the FP station located in the center of the bridge. This proximity between the frequencies of the stations in the stripes (BP and DP) and the bridge frequency indicates constructive (or in-phase) interference of vertical motion at these two points. On the other hand, the minimum of 1.72 Hz in the FP station suggests destructive vertical motion interference (or disfasing) (Özcebe et al., 2020). To determine the direction in which the bridge frequency contributes to the HVSR response, we explored this by rotating the horizontal components in a range of 180 degrees. Figure 5a shows the HVSR curves of the stations on the bridge straps for a rotation angle of 37 degrees, in a direction almost parallel to the Circuito Interior Avenue and perpendicular to the Reforma Avenue. In this figure, we note that the HVSR spectra reach an average amplification of 8, slightly higher than the one observed in Fig. 4, and the site frequency (1.14 Hz) and the maximum spectral order of 1.64 Hz can be clearly distinguished in the BP and DP stations. In Figure 5a, we also plot the spectral ratio of FP central bridge station, which shows no significant changes. In Figure 5b, we show the HVSRs of these same stations for an angle rotation of 115 degrees. At this angle, the BP and DP stations do not show the contribution of the vibration frequency of the bridge, and it

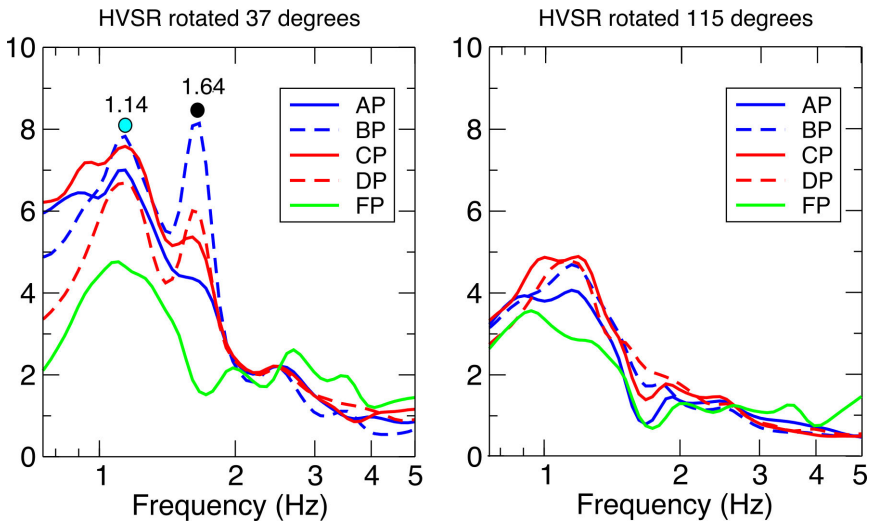

Figure 5. HVSRs rotated in stations over the bridge. The cyan color circle indicates the site frequency (1.14 Hz). The black circle indicates a frequency probably induced by the combination of bridge vibration in the vertical direction and probably a torsional mode.

is more complicated to determine the site frequency. However, the AP, CP, and FP stations clearly show a minimum frequency of the bridge (1.72 Hz), indicating a destructive interference point in the rotation direction of 115 degrees.

The fundamental mode frequency of the bridge is 1.72 Hz, which is very close to the second spectral maximum of 1.64 Hz observed in the HVSR of the BP and DP points. Additionally, the value of 1.72 Hz corresponds to the minimum HVSR curve of the FP station located in the center of the bridge. This proximity between the frequencies of the stations in the stripes (BP and DP) and the bridge frequency indicates constructive (or in-phase) interference of vertical motion at these two points. On the other hand, the minimum of 1.72 Hz in the FP station suggests destructive vertical motion interference (or disfasing) (Özcebe et al., 2020). To determine the direction in which the bridge frequency contributes to the HVSR response, we explored this by rotating the horizontal components in a range of 180 degrees. Figure 5a shows the HVSR curves of the stations on the bridge straps for a rotation angle of 37 degrees, in a direction almost parallel to the Circuito Interior Avenue and perpendicular to the Reforma Avenue. In this figure, we note that the HVSR spectra reach an average amplification of 8, slightly higher than the one observed in Fig. 4, and the site frequency (1.14 Hz) and the maximum spectral order of 1.64 Hz can be clearly distinguished in the BP and DP stations. In Figure 5a, we also plot the spectral ratio of FP central bridge station, which shows no significant changes. In Figure 5b, we show the HVSRs of these same stations for an angle rotation of 115 degrees. At this angle, the BP and DP stations do not show the contribution of the vibration frequency of the bridge, and it is more complicated to determine the site frequency. However, the AP, CP, and FP stations clearly show a minimum frequency of the bridge (1.72 Hz), indicating a destructive interference point in the rotation direction of 115 degrees.

5. Shear wave profiling from seismic interferometry

Seismic Interferometry (SI) is a technique in which a new seismic response is created by correlating the seismic motion recorded in two observations. Developments in acoustics (e.g., Derode et al., 2003) and seismology (Campillo and Paul, 2003) show that such correlation extracts the so-called Green function; the response of the medium that would be recorded in one station as if an impulsive force were applied to the other station or vice versa (virtual source). Using ambient seismic noise to recover the Green function between receivers has been very popular in recent years. Lobkis and Weaver (2001) show that the modal representation of the correlation pulse (diffuse wave field within an elastic medium) has dispersion properties. Shapiro and Campillo (2004) show that coherent Rayleigh waves can be extracted from environmental seismic noise, and their dispersion characteristics can be measured over a wide range of periods. On the one hand, the identification of the travel time (maximum of the correlation pulse) between the pair of receivers can then be used to produce a tomography image that provides the distribution of the velocity medium separating two receivers (e.g., Cárdenas-Soto et al., 2016; 2021). On the other

hand, the configuration of virtual source sections allows spectral analysis of surface waves to form 2D sections of Vs (e.g., Chávez-García et al., 2016).

In this study, we have taken advantage of the different arrays of vertical geophones to explore in detail the subsoil velocity structure. In the first step, we preprocessed the seismic noise records to keep them stationary. Recommended operations are 1-bit decimation and spectral whitening (Bensen et al., 2007). Subsequently, over an hour of recording, we obtained the stacking of 900 cross-correlations derived from 4 s time windows between each pair of receivers. In Figure 6a, we show a virtual source section (Bakulin and Calvert, 2006; Sneider et al., 2006), the cross-correlation of the receiver 01 with the remaining records of the 48 receivers, corresponding to the L2 array. This figure shows that wave trains whose wavelength and amplitude are notable in time delays less than zero are emerging (non-causal part). In a time of greater than zero, the emergence of the causal part of the Green function is not observed. A similar distribution of diffractive noise sources around two receptors, or at the ends of the array, would allow the causal and non-causal part of the Green function to be obtained (Wapenaar and Fokkema, 2006). The correlograms in Fig. 6a show that the symmetry of the correlations is not obtained. This feature is recurrent in the other 48 virtual source sections. This can be attributed to the fact that the distribution of noise sources generated by vehicle flow from the main avenues of the area does not have a preferential orientation with seismic arrays.

Figure 6 shows three examples of virtual source sections for L2 array. We have highlighted the Rayleigh-type surface waves, which emerge dominantly because of a linear array. (Fig. 6a and 6c). In Fig. 6c, whose virtual source is the geophone 48, retro-dispersed surface waves are observed from the position of the geophone 40. The average velocity of these waves is like direct waves, 90 m/s, but their emergence is attractive if they are used as depth object detectors (Schwenk et al., 2016). We hypothesize that the object that could be in that position is a significant water supply pipeline. However, there needs to be public information about it. For the three virtual source examples in Fig. 6, we can observe a high-frequency pulse we identified with a body wave whose velocity matches the P wave-velocity (285 to 380 m/s) on the site (TGC, 2010).

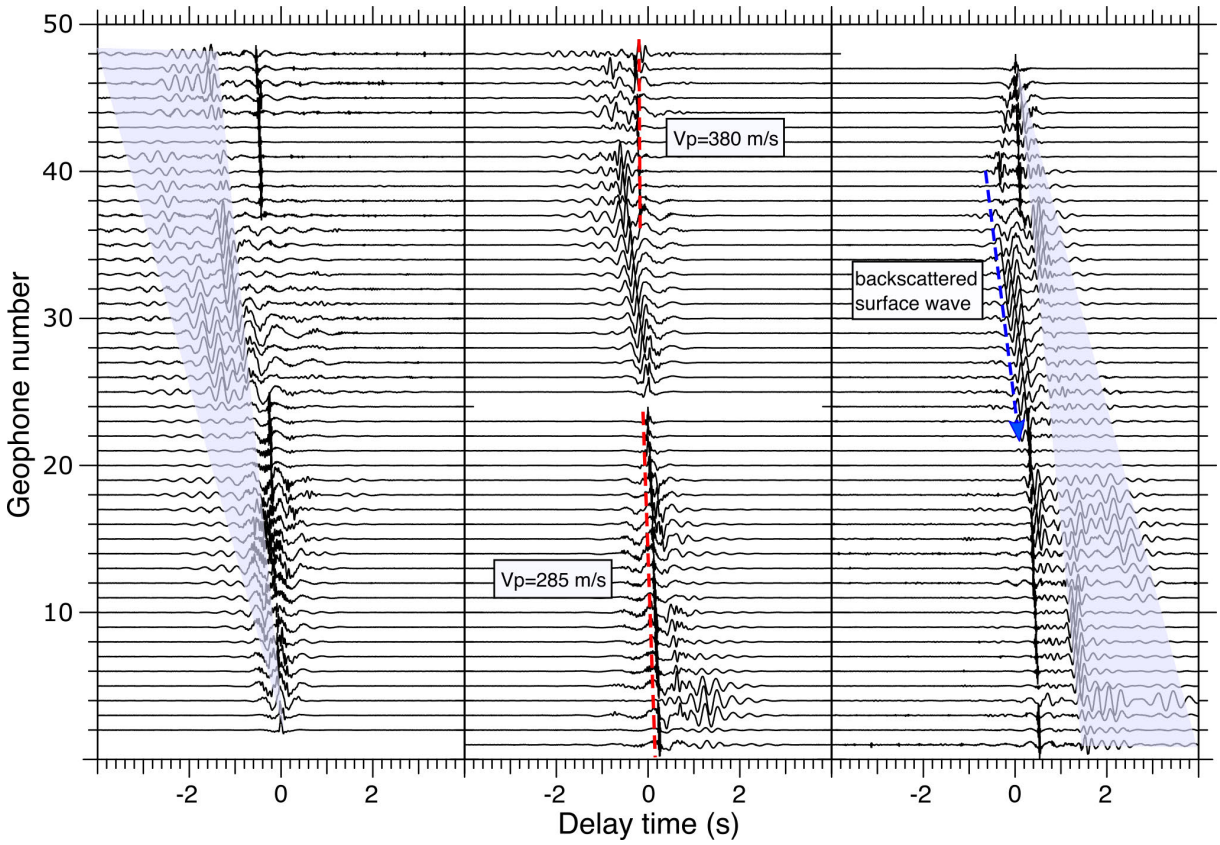

Figure 6. Virtual source seismic sections obtained by cross-correlating receivers: (a) 01, (b) 24, and (c) 48, with respect to the remaining 48 receivers of A2 array. The highlighted areas point to the predominance of Rayleigh-type surface waves. The discontinuous blue line represents a backscattered wave in receiver 40 caused by the virtual source at position 48. The discontinuous red line indicates the presence of P waves and their velocity.

The SI method, which involves the cross-correlation of seismic noise recorded between station pairs, is a crucial tool in understanding the subsoil velocity structure. This method is particularly valuable for identifying the emergence of surface waves. A common practice to obtain a robust dispersion curve is to stack the acausal and causal parts of the Green function (Shapiro and Campillo, 2004; Yang et al., 2023). However, this procedure can alter the amplitude and phase properties if these parts are partially symmetrical and if the stacking is carried out throughout the frequency band. It is important to note that this procedure is appropriate if the emergence of the Green function is the product of cross-correlations of several log time windows (Cárdenas et al., 2016; Chávez-García and Yokoi, 2016).

In order to show that the waveforms of cross-correlations of seismic noise define surface waves, we have calculated the dispersion diagrams for the virtual source sections along the A2 array. In this procedure, we stacked the acausal part with the causal part and subsequently calculated the dispersion diagram using the FTAN technique (Herrmann 2013). Figure 7a shows the frequency vs phase velocity diagram for the virtual source 35 of the array A3, whose dispersion maxima are predominant in the 1 to 10 Hz band. Although the frequency response of the geophones is 4.5 Hz, it is observed that data processing allows the recovery of dispersion maxima at lower frequencies. However, between 1 and 2.5 Hz, the site effects (see Fig. 3) produce great uncertainty in the location of these peaks, which indicate the substratum velocity is 300 to 400 m/s. The velocity in the most surface layers (90 to 150 m/s) is defined by the maximum between 2.5 and 10 Hz. At frequencies greater than 10 Hz, it is impossible to set maximum dispersion due to high attenuation caused by the unconsolidated clay of the site (Ramos-Martínez et al., 1997).

Figure 7b shows the maximum dispersion of all virtual source sections of the A2 array. Although maxima are observed could define the existence of higher modes, the trend of all maxima defines the dispersion curve associated with the Rayleigh fundamental wave mode. This dispersion curve is a key indicator of the subsoil structure. In our case, it indicates that the subsoil model comprises a surface layer with Vs velocity close to 100 m/s that override a more competent substructure with Vs values close to 400 m/s. This structure aligns with the geotechnical description of the subsoil in the Estela de Luz monument (TGC, 2010), confirming the reliability of our methodology and results.

The use of active-source surface waves to determine the Vs structure of the subsoil is a precise and reliable process, carried out daily using the MASW multi-channel surface wave analysis method (Park, 2008; Xia et al., 2009). The acquisition design using this method allows for improved the lateral velocity resolution, ensuring accurate results. In the case of surface waves obtained from the cross-correlation of ambient seismic noise records, we practically have a high density of virtual source sections where the MASW method can be perfectly applied, and that has currently derived in the IMASW or AMASW method (O'Connell and Turner, 2011; Le Feuvre et al., 2015; Cheng et al., 2015; Lontsi et al., 2016; Pan et al., 2016). The definition of the velocity structure depends on the high S/N ratio, and that both the correlation pulse represents a surface wave. An additional method in surface wave

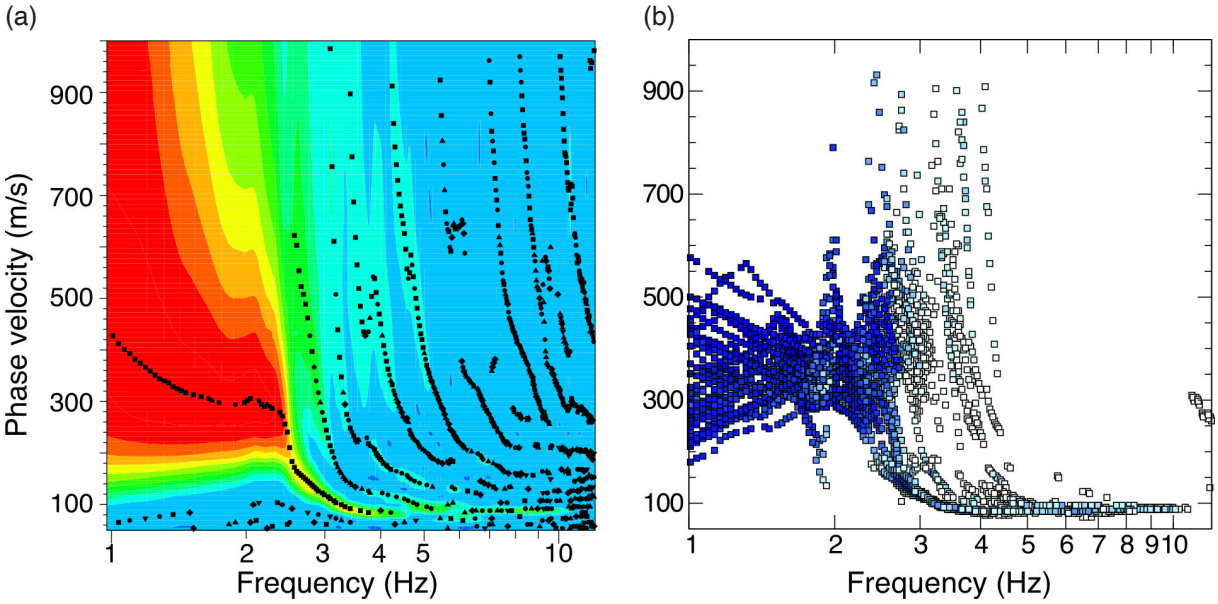

Figure 7. Maximum values of the dispersion diagrams obtained from all virtual source sections. (a) Values of virtual source sections along A3 array. (b) The intense blue color of the small circles indicates the maximum normalized value, and the near-white color indicates 50% of that maximum.

processing, which significantly increases lateral resolution, is the Common Mid-Point Crosscorrelation CMPCC method (Hayashi and Suzuki 2004; Chávez-García and Yokoi, 2016; Ikeda and Tsuji, 2016; Andajani et al., 2019; Pasquet et al., 2021). This method combines the MASW method and cross-correlations between common middle point traces, improving signal-to-noise ratio and highlighting phase-to-phase coherence, further enhancing the precision of our results.

We then exploit the virtual source sections of each of the arrays to create profiles and, subsequently, sections from Vs using the CMPCC method. To ensure the accuracy of our results, we used the software Surface Plus by Geogiga (http://www.geogiga.com, version 9.3), known for its effectiveness in estimating the dispersion curve and the associating shear wave velocity profile. Here, we combined the correlations of the virtual source sections into groups of five traces to extract the dispersion curves. Figure 8 shows the dispersion curves obtained by the CMPCC method along the array A2, and the figure also includes the shear velocity profiles solved by the inversion. The inversion process is carried out by genetic algorithms (GA), a type of global-search optimization strategy ideal for non-linear multi-modal problems due to their low sensitivity to local minima/maxima. Like other heuristic methods, GA explores and evaluates solutions inside a user-defined space. Unlike linear approaches, they do not require a refined starting model that could lead to an incorrect solution due to local minima or maxima (Dal Moro et al., 2007).

GA inversion adopts search space boundaries to simulate conditions without prior information, with many layers and broad velocity and thickness boundaries. In our inversion, we impose an initial model of 11 layers with a constant thickness of 3 m, whose velocities were adjusted and determined by the upper and lower limits of the velocity values of the dispersion curves. The maximum depth reached is based on the dispersion curve form and $\lambda/2$ rule of thumb (Xia et al., 2009). In Figure 8, we can see the resulting 1D models of the dispersion curves inversion (the curve fitness was accepted with an error of less than 10%), which overlap the models, and where it is observed that virtually in all positions, it was possible to obtain a velocity model except for the position 95 m.

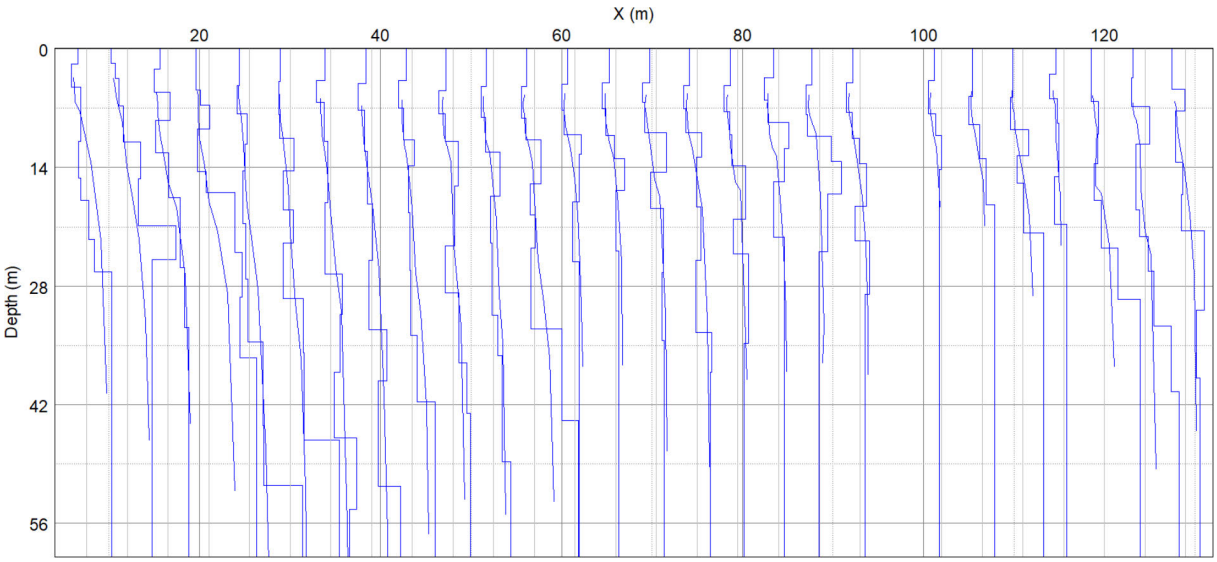

Figure 8. Dispersion curves recovered by the CMPCC method applied to virtual shot gathers of the array A2, and their 1D velocity models.

The seismic sections obtained using the CMPCC method are shown in Fig. 9. The average depth we could resolved is 40 meters, and three layers with noticeable lateral velocity variations can be identified. The first layer, with an average Vs velocity of 100 m/s, consists of unconsolidated clay deposits at the site. In the NE part of the bridge (arrays A1 and A3), this layer is approximately 8 to 12 meters deep, while in the A2 array, it can reach up to 20 meters deep.

The shear wave velocity model of A1 array can be described based on three linear parts formed by the geophones: 01-16, 16-46, and 46-72. A layer of significant irregularity with velocity greater than 300 m/s is observed along each linear section. At the beginning of the line (geophone 01), the depth of this layer is approximately 12 m, and at the end, it is almost 48 m. Near geophone 16, mean velocity values of 300 m/s are observed, which seem to fill the subsoil to a depth of 40 meters. The irregularity of the velocity structure is most evident between geophones 16 and 46.

In this area, which is the NE strip of the bridge, velocities close to 230 m/s are observed, exceeding the average velocity (100 m/s) at depths less than 12 meters. Beneath this structure is a slight inversion of velocity at a depth of 16 meters, and irregularly distributed velocities (ranging from 300 to 400 m/s) up to 44 meters deep. Between geophones 46 and 72 (at the end of the line), values below 300 m/s prevail to a depth of 36 meters.

6. Conclusions

In this study, we have characterized the seismic response around the Bridge of the Lions. This structure serves as a pedestrian passage for hundreds of people who daily see the Forest of Chapultepec in Mexico City, and whose straps rest on two artificially slopes. The results explain the deterioration of the structural elements of the bridge due to the local terrain subsidence, which according to geotechnical studies is a sequence of lake materials whose firm layer is located at an average depth of 23 m.

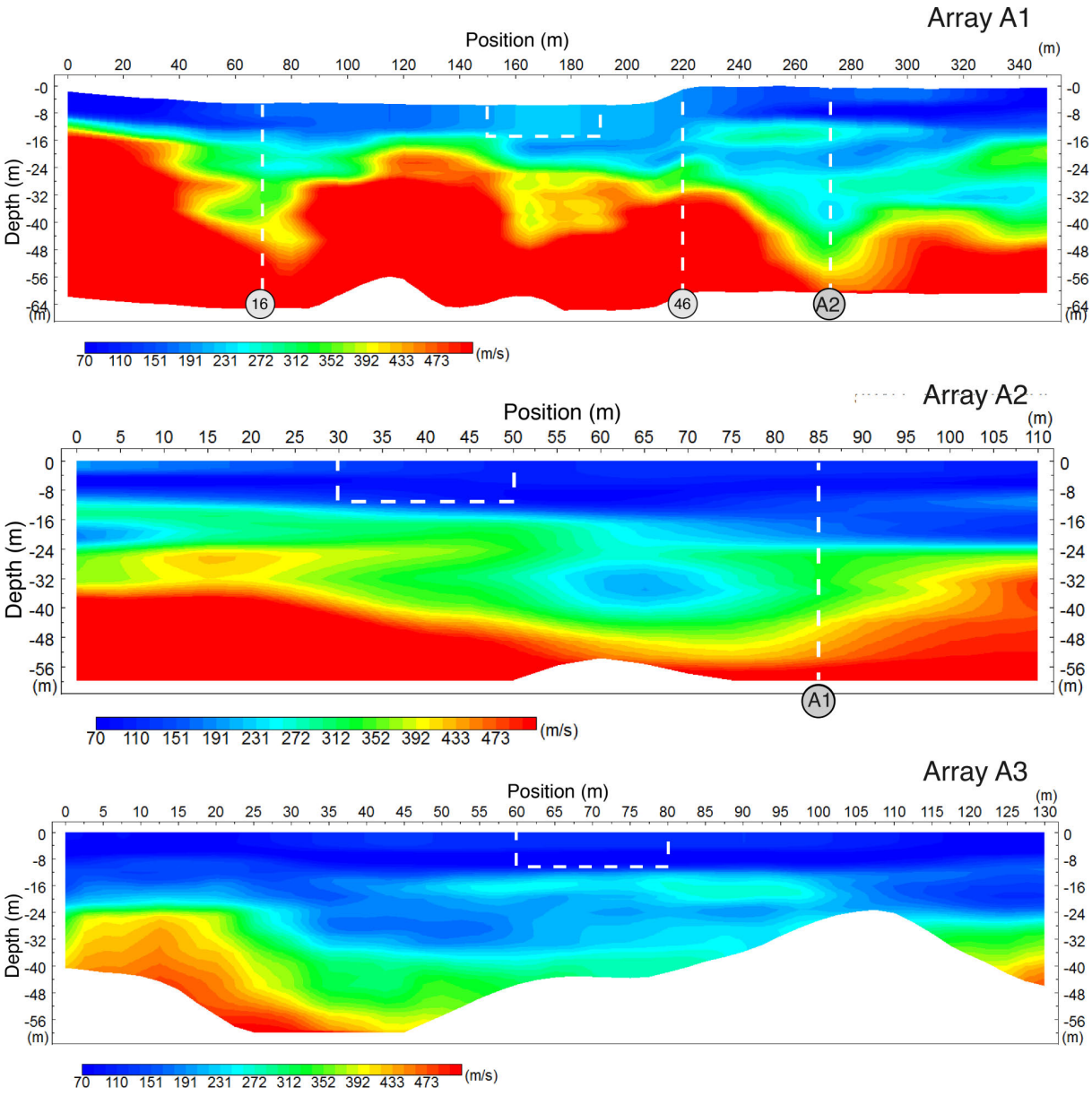

Figure 9. Shear wave velocity sections from CMPCC method applied to virtual sections of each array. The continuous vertical lines in array A1 indicate the limits to where the array is linear. The discontinuous lines in the array A1 and A2 indicate the position where they cross each other. The rectangular-shaped discontinuous lines show where the bridge ribs rest.

The vibration analysis of the bridge straps showed that the frequency of the site, measured in the free field (1.14 Hz), is like the estimated on the straps, which indicates that the depth of the strap does not reach the firm layer. We observe that the bridge vibrates with greater amplitude in the vertical direction at a fundamental frequency of 1.72 Hz. The proximity of this frequency to site frequencies suggests that the bridge may experience soil-structure interaction effects. Also, the rotating analysis of HVSR functions in the bridge straps, shows that there is a second peak in the frequency of 1.64 Hz produced by the contribution of vibration due to the vehicle flow of the Circuito Interior avenue.

The spectral analysis of the surface waves of the virtual source sections generated by the Seismic Interferometry method shows that the surface materials of the subsoil have velocities similar to the soft clays of the lake area (< 150 m/s). A second sequence of consolidated clays (Vs approximately 350 m/s) is evenly distributed in the area, but their geometry is highly irregular where greater damage to the bridge structure is observed. The bridge foundations likely do not penetrate the most competent deep strata, and the existence of soil-structure interaction effects suggest that additional research is necessary to analyze the static and seismic response of the bridge.

Data availability statement. Plots were made using Grace software (https://plasma-gate.weizmann.ac.il/Grace/), and data processing was carried out with Seismological Analysis Tools (version 102.0, https://ds.iris.edu/ds/nodes/dmc/software/downloads/sac/), Computer Programs in Seismology 3.30 (version V1.1.61, https://www.eas.slu.edu/eqc/eqcsoftware.html), and Surface Plus Module by Geogiga (version 9.3, http://www.geogiga.com). The datasets generated during the current study are available from the corresponding author on reasonable request

Acknowledgements. We are grateful to two anonymous reviewers and the editor for their insightful comments and corrections, which significantly enhanced this work. We thank the Chapultepec Forest authorities for facilitating the field work and the CONACYT-GDF Joint Fund (Project 121119). This study was sponsored by UNAM-DGAPA projects: PAPIIT IN108124, PAPIME PE111524.

References

Andajani, R. D., T. Ikeda and T. Tsuji (2019). Surface wave analysis for heterogeneous geological formations in geothermal fields: effect of wave propagation direction, Explor. Geophys., 50, 3, 255-268, doi:10.1080/08123985.2019.1597497.

Anochikwa, C. I., G. van der Kamp and S. L. Barbour (2012). Interpreting pore-water pressure changes induced by water table fluctuations and mechanical loading due to soil moisture changes, Can. Geotech. J., 49, 3, 357-366, doi:10.1139/t11-106.

Auvinet, G., E. Méndez and M. Juárez (2013). Soil Fracturing Induced by Land Subsidence in Mexico City, Proc. 18th Int. Conf. Soil Mech. Geotech. Eng., Paris, France, 2921-2924.

Auvinet, G., E. Méndez and M. Juárez (2017). Recent information on Mexico City subsidence, Proc. 19th Int. Conf. Soil Mech. Geotech. Eng., Seoul, Korea, 2017-September, 3295-3298.

Avilés, J. and L. E. Pérez-Rocha (2010). Regional subsidence of Mexico City and its effects on seismic response, Soil Dyn., Earthq. Eng., 30, 981-989, doi:10.1016/j.soildyn.2010.04.009.

Bakulin, A. and R. Calvert (2006). The virtual source method: Theory and case study, Geophysics, 71, 139-150, doi:10.1190/1.2216190.

Bensen, G. D, M. H. Ritzwoller, M. P. Barmin, A. L. Levshin et al. (2007). Processing seismic ambient noise data to obtain reliable broad-band surface wave dispersion measurements, Geophys. J. Int., 169, 3, 1239-1260, doi:10.1111/j.1365-246X.2007.03374.x.

Bonnefoy-Claudet, S., F. Cotton and P. Y. Bard (2006). The nature of noise wavefield and its applications for site effects studies: A literature review, Earth Sci. Rev., 79, 3-4, 205-227, doi:10.1016/j.earscirev.2006.07.004.

Bonnefoy-Claudet, S., A. Köhler, C. Cornou, M. Wathelet et al. (2008). Effects of Love Waves on Microtremor H/V Ratio, Bull. Seismol. Soc. Am., 98, 1, 288-300, doi:10.1785/0120070063.

Cabral-Cano, E., T. H. Dixon, F. Miralles-Wilhelm, O. Díaz-Molina et al. (2008). Space geodetic imaging of rapid ground subsidence in Mexico City, Bull. Geol. Soc. Am., 120, 11-12, 1556-1566, doi:10.1130/B26001.1.

Campillo, M. and A. Paul (2003). Long range correlations in the diffuse seismic coda, Science, 299, 547-549, doi:10.1126/science.1078551.

Cárdenas-Soto, M., H. Ramos-Saldaña and M. C. Vidal-García (2016). Interferometría de ruido sísmico para la caracterización de la estructura de velocidad 3D de un talud en la 3ª Sección del Bosque de Chapultepec, Ciudad de México, Boletín Soc. Geol. Mex., 68, 2, 173-186.

Cárdenas-Soto, M., J. Piña-Flores, D. Escobedo-Zenil and M. C. Vidal-Garcia (2021). Seismic ambient noise tomography to retrieve near-surface properties in soils with significant 3D lateral heterogeneity: the case of Quinta Colorada building in Chapultepec, Mexico, Nat. Hazards, 108, 1, 129-145, doi:10.1007/s11069-021-04735-4.

Chávez-García, F. J. and T. Yokoi (2016). High lateral resolution exploration using surface waves from noise records, Explor, Geophys., 47, 2, 123-132, doi:10.1071/EG15020.

Cheng, F., J. Xia, Y. Xu, Z. Xu et al. (2015). A new passive seismic method based on seismic interferometry and multichannel analysis of surface waves, J. Appl. Geophys., 117, 126-135, doi:10.1016/j.jappgeo.2015.04.005.

Cigna, F. and D. Tapete (2021). Present-day land subsidence rates, surface faulting hazard and risk in Mexico City with 2014-2020 Sentinel-1 IW InSAR, Remote Sens. Environ., 253, 112161, doi:10.1016/j.rse.2020.112161.

Dal Moro, G., M. Pipan and P. Gabrielli (2007). Rayleigh wave dispersion curve inversion via genetic algorithms and marginal posterior probability density estimation, J. Appl. Geophys., 61, 1, 39-55, doi:10.1016/j.jappgeo.2006.04.002.

Derode, A., E. Larose, M. Tanter, J. De Rosny et al. (2003). Recovering the Green's function from field-field correlations in an open scattering medium (L), J. Acoust. Soc. Am., 113, 6, 2973-2976, doi:10.1121/1.1570436.

Durazo, J. and R. N. Farvolden (1989). The groundwater regime of the Valley of Mexico from historic evidence and field observations, J. Hydrol., 112, 1-2, 171-190, doi:10.1016/0022-1694(89)90187-X.

Figueroa-Miranda, S., J. Tuxpan-Vargas, J. A. Ramos-Leal, V. M. Hernádez-Madrigal et al. (2018). Land subsidence by groundwater over-exploitation from aquifers in tectonic valleys of Central Mexico: a review, Eng. Geol., doi:10.1016/j.enggeo.2018.09.023.

Galloway, D. L., K. W. Hudnut, S. E. Ingebritsen, S. P. Phillips et al. (1998). Detection of aquifer system compaction and land subsidence using interferometric synthetic aperture radar, Antelope Valley, Mojave Desert, California, Water Resour. Res., 34, 10, 2573-2585, doi:10.1029/98WR01285.

Gobierno de México (2022). Plataforma Geocientífica para el Bosque de Chapultepec, http://chapultepec.centrogeo.org.mx/cms/ChapultepecGeo.

Hayashi, K. and H. Suzuki (2004). CMP cross-correlation analysis of multi-channel surface-wave data, Explor. Geophys., 35, 1, 7-13, doi:10.1071/EG04007.

Herrmann, R. B. (2013). Computer programs in seismology: An evolving tool for instruction and research, Seismol. Res. Lett., 84, 6, 1081-1088, doi:10.1785/0220110096.

Ikeda, T. and T. Tsuji (2016). Surface wave attenuation in the shallow subsurface from multichannel-multishot seismic data: a new approach for detecting fractures and lithological discontinuities, Earth Planets Space, 68, 1, 1-14, doi:10.1186/s40623-016-0487-0.

Konno, K. and T. Ohmachi (1998). Ground-Motion Characteristics Estimated from Spectral Ratio between Horizontal and Vertical Components of Microtremor, Bull. Seismol Soc. Am, 88, 1, 228-241, doi:10.1785/BSSA0880010228.

Le Feuvre, M., A. Joubert, D. Leparoux and P. Cote (2015). Passive multi-channel analysis of surface waves with cross-correlations and beamforming, Application to a sea dike, J. Appl. Geophys., 114, 36-51, doi:10.1016/j.jappgeo.2014.12.014.

Lee, W. K., M. Celebi, M. I. Todorovska, H. Igel et al. (2009). Introduction to the special issue on rotational seismology and engineering applications, Bull. Seismol. Soc. Am., 99, 2B, 945-957, doi:10.1785/0120080344.

Lermo, J. and F. J. Chávez-García (1993). Site effect evaluation using spectral ratios with only one station, Bull. Seismol. Soc. Am., 83, 5, 1574-1594, doi:10.1785/BSSA0830051574.

Lobkis, O. I. and R. L. Weaver (2001). On the emergence of the Green's function in the correlations of a diffuse field, J. Acoust. Soc. Am., 110, 6, 3011-3017, doi:10.1121/1.1417528.

Lontsi, A. M., M. Ohrnberger and F. Krüger (2016). Shear wave velocity profile estimation by integrated analysis of active and passive seismic data from small aperture arrays, J. Appl. Geophys., 130, 37-52, doi:10.1016/j.jappgeo.2016.03.034.

Martínez-González, J. A., J. Lermo, E. Ismael, J. Angulo et al. (2011). Efectos del hundimiento regional en los cambios de periodo dominante del suelo en la Cuenta de México: propuesta de nuevos mapas para las Normas Técnicas

Complementarias para Diseño por Sismo (NTCDS), Proc. XVIII Congr. Nac. Ing. Sísmica, Aguascalientes, Ags., Mexico.

Mortagi, M. and J. Ghosh (2020). Climate change considerations for seismic vulnerability assessment of aging highway bridges, ASCE-ASME J. Risk Uncertainty Eng. Syst., Part A, Civil Eng., 6, 1, 04020005, doi:10.1061/AJRUA6.0001038.

Motagh, M., R. Shamshiri, M. Haghshenas, H. U. Haghighi et al. (2017). Quantifying groundwater exploitation induced subsidence in the Rafsanjan plain, southeastern Iran, using InSAR time-series and in situ measurements, Eng. Geol., 218, 134-151, doi:10.1016/j.enggeo.2017.01.011.

Nakamura, Y. (1989). A Method for Dynamic Characteristics Estimation of Subsurface using Microtremor on the Ground Surface, RTRI Res. Rept., 30,1, 25-33.

Ovando-Shelley, E., M. O. Pinto Oliveira, E. Santoyo Villa, V. Hernández et al. (2008). Mexico City: Geotechnical Concerns in the Preservation of Monuments, Int. J. Archit. Herit, 2, 1, 60-82, doi:10.1080/15583050701612887.

O'Connell, D. R. and J. P. Turner (2011). Interferometric multichannel analysis of surface waves (IMASW), Bull. Seismol. Soc. Am., 101, 5, 2122-2141, doi:10.1785/0120100230.

Özcebe, A. G., C. Smerzini and V. Bhanu (2020). Insights into the effect of spatial variability of recorded earthquake ground motion on the response of a bridge structure, J. Earthquake Eng., 24, 6, 920-946, doi:10.1080/13632469.2018.1453412.

Özşahin, E. and G. Pekcan (2019). Effect of torsional ground motion on the seismic response of highway bridges, Bull. Earthquake Eng., 17, 2603-2625, doi:10.1007/s10518-018-00550-8.

Park, C. (2008). Imaging dispersion of passive surface waves with active scheme, Symp. Appl. Geophys. Eng. Environ. Prob. Philadelphia, doi:10.3997/2214-4609-PDB.177.48.

Pan, Y., J. Xia, Y. Xu, Z. Xu et al. (2016). Delineating shallow S-wave velocity structure using multiple ambient-noise surface-wave methods: An example from Western Junggar, China, Bull. Seism. Soc. Am., 106, 2, 327-336, doi:10.1785/0120150014.

Pasquet, S., W. Wang, P. Chen and B. A. Flinchum (2021). Multiwindow weighted stacking of surface-wave dispersion, Geophysics, 86, 2, EN39-EN50, doi:10.1190/GEO2020-0096.1.

Ramos-Martínez, J., F. J. Chavez-Garcia, E. Romero-Jimenez and J. L. Rodriguez-Zuniga (1997). Site effects in Mexico City: constraints from surface wave inversion of shallow refraction data, J. Appl. Geophys, 36, 4, 157-165, doi:10.1016/S0926-9851(96)00057-2.

Romo, O. M., M. Mendoza, E. Botero and O. Flores (2012). Estudios para la verificación de la seguridad estructural y geotécnica del monumento del Bicentenario de la Independencia de México: "Estela de Luz". Aspectos geotécnicos, Informe Final del Instituto de Ingeniería, UNAM para la empresa I.I.I. Servicios S.A. de C.V., abril.

Shapiro, N. M. and M. Campillo (2004). Emergence of broadband Rayleigh waves from correlations of the ambient seismic noise, Geophys. Res. Lett., 31, 7, doi:10.1029/2004GL019491.

Shelley, E. O. (2011). Some geotechnical properties to characterize Mexico City Clay, in 14th Pan-American Conference on Soil Mechanics and Geotechnical Engineering, 64th Canadian Geotechnical Conference, October 2-6, 2011, Toronto, Ontario, Canada.

Schwenk, J. T., S. D. Sloan, J. Ivanov and R. D. Miller (2016). Surface-wave methods for anomaly detection, Geophysics, 81, 4, EN29-EN4, doi:10.1190/GEO2015-0356.1.

Snieder, R., J. Sheiman and R. Calvert (2006). Equivalence of the virtual source method and wavefield deconvolution in seismic interferometry, Phys. Rev., E 73, 066620, doi:10.1103/PhysRevE.73.066620.

Tarantino, A. and E. De Col (2008). Compaction behaviour of clay, Géotechnique, 58, 3, 199-213, doi:10.1680/geot.2008.58.3.199.

TGC Geotecnia (2010). Estudio geotécnico para la revisión de la solución de la cimentación del monumento conmemorativo del Bicentenario del Inicio de la Independencia Nacional, en el D.F., primera etapa, Mayo.

Tuan, T. T., F. Scherbaum and P. G. Malischewsky (2011). On the relationship of peaks and troughs of the ellipticity (H/V) of Rayleigh waves and the transmission response of single layer over half-space models, Geophys. J. Int., 184, 2, 793-800, doi:10.1111/j.1365-246X.2010.04863.x.

Wapenaar, K. and J. Fokkema (2006). Green's function representations for seismic interferometry, Geophysics, 71, 4, SI33-SI46, doi:10.1190/1.2213955.

Wathelet, M., D. Jongmans, M. Ohrnberger and S. Bonnefoy-Claudet (2008). Array performances for ambient vibrations on a shallow structure and consequences over Vs inversion, J. Seismol., 12, 1-19, doi:10.1007/s10950-007-9067-x.

Xia, J., R. D. Miller, Y. Xu, Y. Luo et al. (2009). High-frequency Rayleigh-wave method, J. Earth Sci., 20, 563-579, doi:10.1007/s12583-009-0047-7.

Yang, X., J., Bryan, K. Okubo, C. Jiang et al. (2023). Optimal stacking of noise cross-correlation functions, Geophys. J. Int., 232, 3, 1600-1618, doi:10.1093/gji/ggac410.

Zhu B. and D. M. Frangopol (2013). Risk-based approach for optimum maintenance of bridges under traffic and earthquake loads, J. Struct. Eng., 139, 3, 422-434, doi:10.1061/(ASCE)ST.1943-541X.0000671.

***CORRESPONDING AUTHOR: Martín CÁRDENAS-SOTO**,
National Autonomous University of Mexico, School of Engineering, Geophysical Department, Mexico City, México
e-mail: martinc@unam.mx